

# Nuclei of early-type dwarf galaxies: insights from stellar populations<sup>\*</sup>

Sanjaya Paudel<sup>1†</sup>, Thorsten Lisker<sup>1</sup>, Harald Kuntschner<sup>2</sup>

<sup>1</sup>*Astronomisches Rechen-Institut, Zentrum für Astronomie der Universität Heidelberg, Mönchhofstr. 12-14, 69120 Heidelberg, Germany*

<sup>2</sup>*Space Telescope European Coordinating Facility, European Southern Observatory, Karl-Schwarzschild-Str. 2, 85748 Garching, Germany*

Accepted ... Received ... ; in original form 10 November 2018

## ABSTRACT

We present a comprehensive analysis of the spatially resolved stellar population properties of 26 early-type dwarf (dE) galaxies in the Virgo cluster. Using Lick/IDS absorption line indices we derive simple stellar population (SSP)-equivalent age, metallicity and  $[\alpha/\text{Fe}]$  abundance ratio. In particular, we focus on the comparison of the stellar populations between the central nucleus and the surrounding galactic main body. The stellar populations of the nuclei are, for most dEs, significantly younger than those of the respective galactic main bodies, with an average difference of 3.5 Gyr. We find only five dEs with significantly older nuclei than their galactic main bodies. Furthermore, we observe most dE nuclei to be more metal rich compared to their host galaxies. These age and metallicity behaviours are shown by almost all dEs brighter than  $M_r = -17$  mag.

The metallicity of both nuclei and galactic main bodies correlates with the total luminosity of the dEs. However, the metallicity of the nuclei covers a larger range (+0.18 to -1.22 dex) than that of the galactic main bodies, which all have sub-solar metallicity. The ages of dE nuclei show a statistically significant correlation with the local projected galaxy density within the cluster, such that younger ages are predominantly observed outside of the high-density central cluster region. The alpha-element abundance ratios are consistent with solar for both nuclei and galactic main bodies.

We also examine the presence of radial gradients in the SSP parameters for a subset of 13 dEs (up to 1.2 kpc or 15 arcsec radius). We notice two different types of gradients, namely smooth profiles that include the nucleus, and profiles where a break occurs between the nucleus and the rest of the galaxy. Nevertheless, an overall trend of increasing age and decreasing metallicity with radius exists, consistent with earlier studies. The  $\alpha$ -abundance ratio as function of radius is consistent with no gradient.

Possible formation scenarios for the nuclei of dEs are discussed. The young and metal-enhanced population of nuclei suggests that these might have formed at later epochs, or the termination of star formation activity in the nuclei might have occurred relatively late, perhaps due to continuous infall of gas into the central potential well. Our stellar population analysis suggests that the merging of globular clusters is not an appropriate scenario for the formation of most dE nuclei, at least not for the brighter dEs. We speculate that there might be different formation processes which are responsible for the formation of dEs and their nuclei depending on their luminosity.

**Key words:** galaxies: dwarf – galaxies: evolution – galaxies: formation – galaxies: stellar content – galaxies: elliptical and lenticular, cD – galaxies: clusters: individual: Virgo

## 1 INTRODUCTION

Early-type dwarf galaxies (dEs,  $M_B > -18$ ) are the numerically dominant population in the present-day Universe (Sandage et al. 1985; Binggeli et al. 1987; Ferguson & Binggeli 1994). They also exhibit strong clus-

<sup>\*</sup> Based on observations collected at the European Organisation for Astronomical Research in the Southern Hemisphere, Chile (programme 078.B-0178)

<sup>†</sup> E-mail: sjy@x-astro.net

tering, being found predominantly in the close vicinity of giant galaxies, either as satellites of individual giants, or as members of galaxy clusters (Ferguson & Sandage 1989). Although the dEs are characterized by their smooth appearance, having no recent or ongoing star formation and apparently no gas or dust content, the understanding of their origin and evolution remain major challenges for extragalactic astronomy. Stellar population studies show that dEs exhibit on average younger ages as compared to their giant counterparts, and also a lower metal content according to the correlation of metallicity and luminosity (Michielsen et al. 2008). However, past studies provided a wide range of ages (e.g., Poggianti et al. 2001; Rakos et al. 2001; Caldwell et al. 2003; Geha et al. 2003; van Zee et al. 2004), from as old as being primordial objects to dEs with recently formed young stellar populations.

It appears that dEs themselves are not a homogeneous class of objects. Sub-structures such as stellar disks, faint spiral arms or bars are quite frequent among the brighter dEs (Lisker et al. 2006, 2007). Many dEs were found to contain a central surface brightness enhancement consistent with a point source on top of the galactic main body (e.g. Binggeli & Cameron 1991, 1993), referred to as so-called nucleated dEs. The studies from the HST/ACS Virgo cluster survey (Côté et al. 2006), with their high angular resolution, not only verified the presence of such a distinct nucleus but also showed that nuclei are ubiquitous in bright dEs, covering a range in nucleus brightness. Interestingly, dEs with comparably faint nuclei that had not been identified before Côté et al. (2006) show several systematically different properties as compared to dEs with bright nuclei (Lisker et al. 2007, 2008).

Different studies of dE nuclei from different data sets found several contradictory properties for the nuclei (Grant et al. 2005; Lotz et al. 2004; Côté et al. 2006). Particularly, the ground and space based data sets yielded different results. Grant et al. (2005) found that the nuclei are on average redder than their surrounding galactic main body. On the other hand, studies using HST observations (Côté et al. 2006; Lotz et al. 2004) measured the dE nuclei to be slightly bluer than the galactic part. Furthermore, Côté et al. (2006), who used high quality data sets from the ACS Virgo Cluster Survey, proposed that the nuclei rather closely match the nuclear clusters of late type spiral galaxies in terms of size, luminosity and overall frequency. Another related scenario is also emerging: the recently discovered new (candidate) type of extremely small dwarf galaxies, the UCDs (Ultra Compact Dwarfs) with typical magnitudes of  $-13 < M_b < -11$  (Hilker et al. 1999; Phillipps et al. 2001), might be the remnant nuclei of tidally stripped dwarf galaxies (Bekki et al. 2003; Drinkwater et al. 2003; Goerdt et al. 2008).

The formation mechanisms of the nuclei of dEs are poorly understood and various possibilities have been proposed, also depending on the evolution and formation of dEs as a whole. As the nucleated dEs are preferentially rounder in shape, van den Bergh (1986) proposed that the nuclei of dEs could have formed from the gas that sank to the centre of the more slowly rotating objects. Since they predominantly appear in highly dense environments, like the centre of a cluster of galaxies, the pressure from the surrounding inter-galactic medium may allow dwarf galaxies to retain

their gas during star formation and produce multiple generation of stars (Silk et al. 1987; Babul & Rees 1992), forming nuclei in the process. In both proposed scenarios the nuclei are formed along with the evolution of the galaxy itself, i.e., continuous star formation activity occurs at the dE centre as time passes. Unlike that, Oh & Lin (2000) suggested that dE nuclei might have formed in a different way, namely through subsequent migration or orbital decay of several globular clusters towards the centre of their host dE.

It is difficult to provide a definitive observational test of these different scenarios for nucleus formation. Nevertheless, we can gain some insight by comparing the different observational properties, in particular relative ages and chemical enrichment characteristics, of the nuclei with their galactic main bodies, as well as with UCDs as their possible descendants. However, we need to bear mind that there may be a mixture of different formation scenarios.

Our previous study based on this dataset (Paudel et al. 2010, hereafter Paper I) has focused on the analysis of the inner stellar populations of dEs as a whole, without separating nuclei and galactic main bodies. Instead, our intention was to see the variation of the inner stellar population properties with different morphological subclasses of dEs (cf. Lisker et al. 2007), using a much larger sample of Virgo dEs than in previous Lick index studies. We showed that dEs with different substructure properties (with/without disk features, Lisker et al. 2006) have significantly different stellar populations: dEs with disk features are younger and more metal rich than dEs without disks. Therefore we concluded that these dEs probably do not have the same origin, as they also differ in their distribution with local environmental density in which they reside. By selection, all dEs in our sample contain a central nucleus, therefore it seems important to see the nature of the stellar populations of the nuclei and the surrounding galactic main bodies separately. And since there are different possibilities for the processes that form nuclei and also dEs themselves, we ask: can the nuclei thus tell us something about the formation history of dEs?

This paper is organized as follows. In Section 2, we describe the sample of Virgo cluster dEs, observation and data reduction in brief. In section 3, we describe the measurement of line-strength indices in the Lick/IDS system. Our main results from the stellar population parameters are given in Section 4 and are discussed in Section 5. Finally, we summarize our findings in Section 6.

## 2 THE SAMPLE, OBSERVATION AND DATA REDUCTION

Our sample comprises 26 nucleated dEs in the Virgo cluster. The sample properties such as position in the color magnitude relation, total galactic luminosity, radial velocity and their local projected density within the Virgo cluster are described in detail in Paper I. The sample covers the full range of local density and includes the different morphological dE subtypes, i.e., 8 dEs with disks (dE(di)s) and 18 dEs without disks, which we hereafter simply refer to as dE(N)s. One dE(di) (VCC0308) contains a weak blue color excess in the centre, thus being referred to as a blue-centre dE (cf. Lisker et al. 2006).

The observations were carried out at the ESO Very

Large Telescope (VLT) with the FORS2 instrument. The 1" slit and 300V grism provide an instrumental resolution of  $\simeq 11$  Å (Full Width at Half Maximum, FWHM). The other basic observational properties and the data reduction processes are described in detail in Paper I.

We carefully checked the issue of scattered light during the reduction of the data, since the presence of a significant amount of scattered light could produce an artificial gradient in the measured line indices. Fortunately, our MOS-MXU setup utilized in this investigation provides the opportunity to quantify it. There are always free intra-slit regions where no light enters directly from the sky. After the bias subtraction these regions should not contain any flux, unless scattered light were present. We thus calculate the average amount of light within such regions manually. We find that the mean is zero within the uncertainties, which are of the order of some hundredths of a count. The FORS2 pipeline reduction produces the same result. It therefore confirms that there is no scattered light left in the spectra.

In a different way, there is still the probability of mixing the nucleus light out to far beyond the central nucleus in case of bad seeing or instrumental blurring. To examine this effect, we also observed a star in an additional slit along with each target-field. Then, through the light profile of this star, we quantify the amount of such light at a radius of 3" beyond the centre. Our measurements show that spread nuclear light is less than 1% of galactic light at 3" distance from the galaxy centre. The observed FWHM of the stars is always  $\sim 1.3''$  or less, consistent with this negligible fraction of starlight at 3" from the centre.

## 2.1 Extraction of nuclear spectra and analysis of light profile

Our goals in this paper are the measurement of simple stellar population (SSP) equivalent parameters (see [Trager et al. 2008](#)) of dE nuclei and a comparison with the SSPs of the surrounding galactic main bodies. Additionally, if the signal-to-noise ratio (hereafter SNR) permits us, we wish to explore gradients in the SSP parameters, which helps to determine whether the SSP of the nuclei is very different from the rest of the galaxy or is just a continuity of a smooth SSP gradient at the centre of dEs. Although there is no precise definition for what a nucleus is, the working definition used by several studies is that an excess of light from the smooth exponential (or higher order Sérsic) profile of the rest of the galactic part is observed, looking like a compact source sitting at the centre of the galaxy. Because of its compactness, it is considered as a point source and represented with a seeing convolved Gaussian light profile. Likewise, the study of [Grant et al. 2005](#) represents the nuclei as a point source convolved with Gaussian seeing. [Côté et al. 2006](#) used a slightly different approach, by fitting a two component core-Sérsic model ([Graham & Guzmán 2003](#)). In Fig. 1 we can clearly see for most dEs the change in the light profile at the centre (e.g. VCC0216, VCC0856, VCC0545, VCC1353 and VCC1945). On the other hand, VCC0308, VCC0990, VCC1261 and VCC1826 exhibit a rather smooth light profile. There may be several factors which produce such differences in the light profile even though all dEs in this sample are confirmed as nucleated from other photometric studies ([Binggeli et al. 1985](#); [Lisker et al. 2007](#)). In-

**Table 1.** Basic parameters and signal-to-noise ratio for our targets.

Galaxy	Nuc.	Gal.	Reff	$M_r$	$m_r$	Light
VCC	(SNR)	(SNR)	arcsec	Total	Nuc	fraction
No.	$\text{pix}^{-1}$	$\text{pix}^{-1}$	arc-sec	mag	mag	in %
0216	47	30	13.3	-16.78	-11.58	22
0308	35	31	18.7	-17.95	-11.91	40
0389	32	30	17.2	-18.00	-12.59	48
0490	32	23	27.6	-18.09	-12.43	25
0545	33	30	13.3	-16.61	-11.71	35
0725	23	—	25.2	-16.19	-10.17	—
0856	56	35	15.9	-17.71	-12.73	23
0929	56	34	20.5	-18.58	-13.13	33
0990	35	33	09.9	-17.39	-12.52	53
1167	46	30	27.3	-16.95	-12.01	17
1185	33	50	19.3	-16.65	-10.76	30
1254	67	31	14.9	-17.17	-13.31	09
1261	50	42	22.5	-18.47	-12.53	42
1304	35	31	16.2	-16.86	-12.23	33
1308	39	27	11.4	-16.50	-11.32	44
1333	41	28	18.5	-15.44	-11.76	10
1348	42	25	13.1	-16.94	-12.83	23
1353	28	31	08.8	-15.51	-10.64	53
1355	24	28	29.6	-17.59	-10.96	57
1389	30	31	12.8	-15.98	-10.78	36
1407	27	31	11.8	-16.95	-10.99	52
1661	34	29	18.9	-16.18	-11.18	16
1826	23	31	07.8	-16.30	-11.91	56
1861	30	31	18.4	-17.78	-11.83	47
1945	31	38	21.5	-17.11	-11.66	35
2019	31	29	18.1	-17.53	-11.34	37

The second and third columns are the measured signal-to-noise ratio (SNR) per pixel at 5000Å for the galactic-light-subtracted nuclear spectra and the galactic main body spectra, respectively. The fourth column gives the half-light semi-major axis in SDSS  $r$  from Lisker07. The fifth and sixth columns are total galactic and nucleus absolute magnitudes in SDSS  $r$ , applying a distance modulus of  $m - M = 31.09$  mag ([Mei et al. 2007](#)), corresponding to  $d = 16.5$  Mpc. The last column represents the amount (in fraction of total light of the central aperture) of light subtracted from the central nucleus spectrum. Nucleus magnitudes were derived as described in [Paudel et al. \(2010\)](#): a two-dimensional elliptical model image of the galaxy, based on a Sérsic fit to the radial profile, was subtracted from the original image, taking into account the median SDSS PSF of  $1.4''$  FWHM. The nucleus magnitude was then measured by circular aperture photometry with  $r = 2''$  centered on the nucleus; the error is estimated to be 0.2 mag.

sufficient spatial resolution or observed seeing which might blur the steeper light profile of the nuclei makes it harder to separate the galactic light profile. However, [Côté et al. \(2006\)](#) have observed the existence of a profile break in the case of VCC0856, VCC1261, VCC1355, VCC1407, VCC1661 and VCC2019, reconfirming the existence of a nucleus at the centre of dEs with HST high resolution surface photometry.

It is rather difficult to carry out an analysis of the stellar populations of nuclei *alone*, because the nuclei are always situated on top of the underlying galactic main bodies. It is also hard to separate the galactic light from the central nucleus of such a faint object. The studies that have been done by [Chilingarian \(2009\)](#) and [Koleva et al. \(2009\)](#) provide results without galactic light subtraction from the

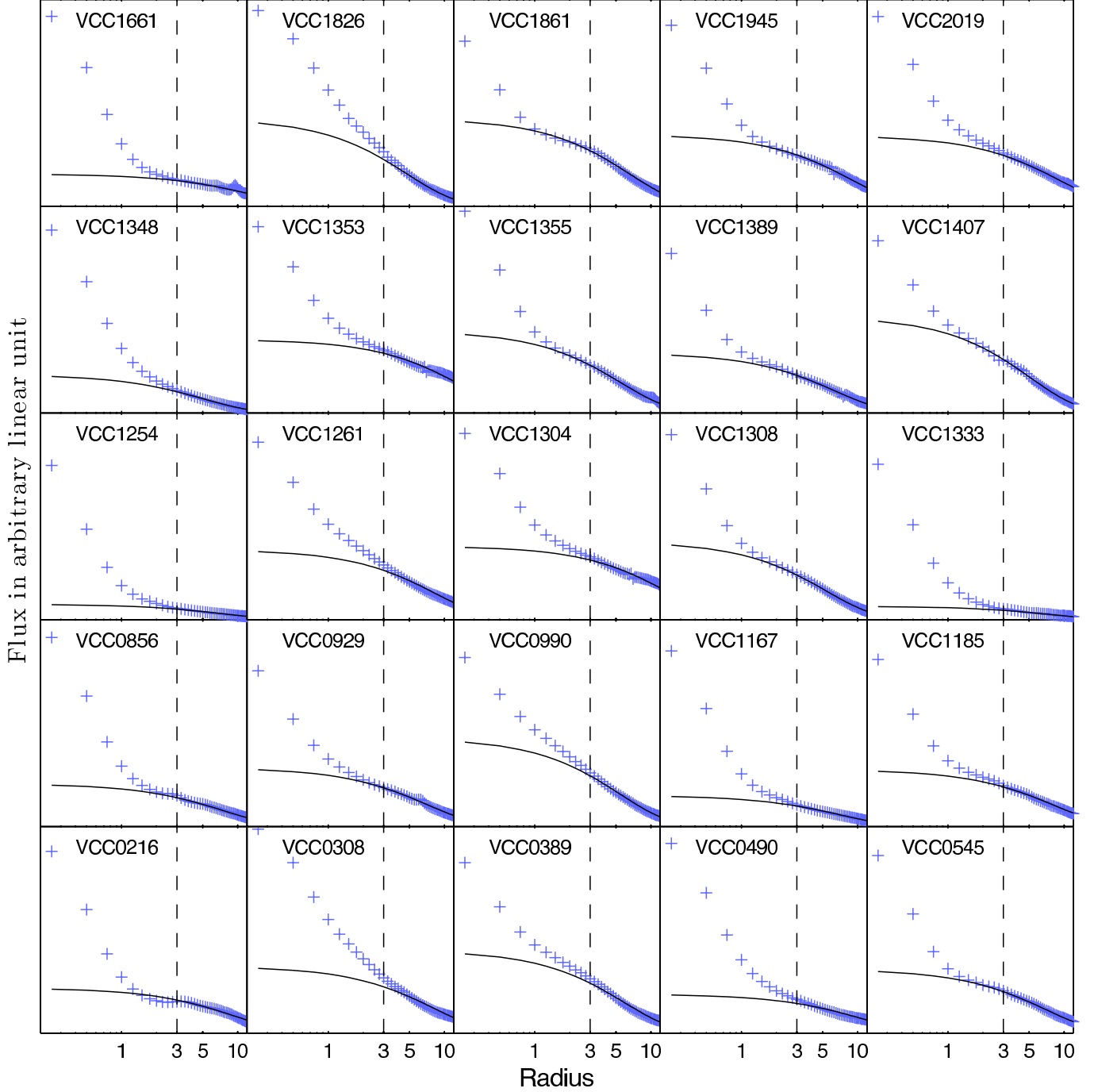


**Figure 1.** The light profile of dEs. The crosses represent the observed flux along the slit, and the solid line is the fitted exponential profile beyond  $3''$  and extrapolated to the centre.

nucleus. Although there is, in our sample, typically a fairly large domination of light from the nucleus as compared to galactic light at the photometric centre of the dEs, still a considerable amount of underlying light of the host galaxy can alter the observed properties of the nuclei. We therefore aim to reduce the galactic light contamination in the nucleus spectra, attempting a separate extraction of spectra for the nucleus and the galactic part.

We extract the nucleus spectra from the central  $0''.75$  (i.e., 3 pixels). The region between  $0''.75$  and  $3''$  is not used

for this extraction, to avoid any effects of nucleus light in the spectra of the galactic main body. We then integrate over the interval  $3''$  to  $8''$  from each side of the nucleus to extract the spectra of the galactic main body (see Appendix A, Fig. A1). The individual spectra of galactic main body from the different side of nucleus were then co-added to produce a spectrum of higher SNR. In order to subtract the galaxy light from the nucleus, we determine a scaling factor by fitting the galactic main body's light profile (measured along the slit) by an exponential profile and extrapolating it to the

very centre, yielding the amount of galaxy light contained in the nucleus aperture (see Appendix A). Given the above considerations about the difficulty of separating nucleus and galaxy, we point out that our approach ensures the removal of a *significant part*, yet probably not 100% of galaxy light contamination. For those few cases where the central light profile looks rather smooth with ground-based data, and can only be disentangled with space-based photometry, our “nucleus” spectrum thus needs to be considered representative for the combination of nucleus *and* galactic central light.

Before co-adding the spectra from the different sides of the galaxies, we analyze their slit profile to check for inconsistencies or asymmetries, e.g. by contaminating objects on the slit. We find only one galaxy, VCC1945, has an asymmetric profile that deviates from a smooth exponential profile on one side. We noticed that a bright point source (foreground/ background or intra-galactic globular cluster) lies on one side of the slit. Therefore, we remove the spectrum from this side. For completeness, we also compare the spectra from the different sides of the galaxy before co-adding them, and we always find good agreement. Finally, the measured SNR at 5000Å for both the galaxy-subtracted nucleus spectra and the combined galaxy spectra is given in Table 1.

### 3 LINE STRENGTH MEASUREMENTS

Before measuring the Lick absorption line indices from the flux calibrated spectra of the galactic main bodies and nuclei, we also carefully checked whether any emission lines are present, particularly since some dEs show a fairly young nucleus. However, we do not detect any [OIII] emission, thus we do not correct the H $\beta$  absorption for possible contamination by emission. If such emission were present, it would make the measured H $\beta$  absorption smaller, and therefore derived ages older. On the other hand, it could be possible that we do not see any emission lines because of the low spectral resolution. To quantify what strength of an emission line in a high-resolution spectrum (i.e. model of Vazdekis et al. 2010) would be smeared out in a low-resolution like ours, such that it is not recognized visually, we select a model spectrum of age 2 Gyr, and added an emission of H $\beta$ . We then degrade the spectrum to the low-resolution of 11 Å. We find that the added emission line could have an effect of up to 12% on the measured absorption line strength, which reveals a relatively small effect on the age.

Note that we have not applied a velocity dispersion correction for the Lick indices, because the expected galactic velocity dispersion,  $\sigma_{gal} \leq 50 \text{ km s}^{-1}$ , is significantly below our spectral resolution  $\sigma_{instr} \sim 280 \text{ km s}^{-1}$ . Therefore these corrections are not necessary.

To measure the absorption line strengths from the spectra, we use the routine *Indexf*<sup>1</sup> developed by N. Cardiel. It uses the definition of the Lick indices from Trager et al. (1998) and also derives the uncertainty in measured strength using Monte-Carlo simulations. Calibrations of our measured line strengths to the actual Lick system have been done as described in Paper I (Section 4.2 and Appendix B

in that paper).

We use the method of Lick indices (Burstein et al. 1984; Worthey et al. 1994; Trager et al. 1998) as a tool for estimating the stellar population characteristics. We translate our Lick index measurements into SSP-equivalent ages, metallicities, and  $\alpha$ -element abundance ratios by comparing them to the stellar population models of Thomas et al. (2003) by  $\chi^2$ -minimization, following Proctor & Sansom (2002). For this we use the nine indices H $\delta_F$ , H $\gamma_F$ , Fe4383, H $\beta$ , Fe5015, Mg *b*, Fe5270, Fe5335 & Fe5406. Note that the SSP models assume all the stars were formed in a single burst and have the same age and metallicity. In fact, the galaxies may be a composite stellar system formed during several episodic star formation events, with different chemical compositions in general. Therefore, our estimated stellar population parameters can be considered *SSP-equivalent stellar populations*. The correlation of age and metallicity in the model fitting is illustrated in Appendix B.

### 4 RESULTS: AGES, METALLICITIES AND ALPHA-ABUNDANCE RATIOS

In this section, we present the SSP-equivalent ages, metallicities and  $\alpha$ -abundance ratios of our sample dEs (Table 2). Note that, in case of the least luminous dE, VCC0725, we find that the sky noise becomes dominant beyond the central aperture. Hence, we remove its galactic part from the sample and therefore provide no SSP parameters for the galactic main body of this dE.

We can clearly see that the ages of the nuclei are significantly lower than the ages of the surrounding galactic main bodies (Fig. 2). The differences are more prominent in the disk dEs: only VCC1304 has a nucleus that is older than the galactic part. Moreover, we find that only four other non-disk dE(N)s (VCC1167, VCC1333, VCC1389 and VCC1661 – see Sec. 2) have nuclei with significantly larger ages than the galactic main bodies. The median difference in age between the galactic main bodies and nuclei is 3.5 Gyr. Examining Fig. 2 individually galaxy by galaxy, one can see that VCC0856 shows the largest difference (>10 Gyr) in age between the nucleus and the galactic part. The nucleus of the blue centre dE VCC0308, while having a young age, does not show up as being special, having an age of  $1.5 \pm 0.1$  Gyr, similar to other dE nuclei such as VCC0216, VCC2019 and VCC1826.

The metallicity distributions of the nuclei and the surrounding galactic main bodies also differ: the majority of the nuclei are relatively metal enhanced as compared to the galactic main bodies. However, it is remarkable that those nuclei that are older or equally old as the galactic part are also less metal rich than the latter. We find that the nucleus of VCC1308 has the highest metallicity of  $+0.16 \pm 0.12$  dex. For all dEs, the galactic main bodies have sub-solar metallicity. The  $\alpha$ -abundance ratio from nuclei and galactic main bodies show a wide distribution. The nuclei of three dEs (i.e., VCC0308, VCC0389 and VCC0545) show significant  $\alpha$ -enhancement as compared to their galactic part. On the contrary, four dEs, VCC0990, VCC0929, VCC1353 and VCC1861, exhibit a significantly enhanced  $\alpha$ -abundance in the galactic part as compared to their nucleus.

<sup>1</sup> <http://www.ucm.es/info/Astrof/software/indexf/indexf.html>



**Table 2.** SSP-equivalent stellar population parameters for the nuclei and the galactic main bodies.

Galaxy Name	Age, Gyr		[Z/H], dex		[ $\alpha$ /Fe], dex	
	Nuc.	Gal.	Nuc.	Gal.	Nuc.	Gal.
VCC0216	1.4 <sup>+0.3</sup> <sub>-0.3</sub>	4.0 <sup>+1.8</sup> <sub>-1.2</sub>	-0.61 ± 0.15	-0.63 ± 0.22	0.09 ± 0.08	0.03 ± 0.18
VCC0308	1.5 <sup>+0.1</sup> <sub>-0.1</sub>	3.6 <sup>+1.6</sup> <sub>-0.9</sub>	0.01 ± 0.10	-0.34 ± 0.17	0.42 ± 0.09	-0.07 ± 0.14
VCC0389	4.1 <sup>+2.1</sup> <sub>-1.3</sub>	9.1 <sup>+3.4</sup> <sub>-1.9</sub>	-0.24 ± 0.17	-0.43 ± 0.20	0.17 ± 0.12	-0.15 ± 0.15
VCC0490	1.9 <sup>+0.7</sup> <sub>-0.2</sub>	3.6 <sup>+2.1</sup> <sub>-1.1</sub>	-0.02 ± 0.22	-0.24 ± 0.17	-0.11 ± 0.11	-0.11 ± 0.15
VCC0545	6.9 <sup>+2.6</sup> <sub>-1.2</sub>	12.5 <sup>+0.0</sup> <sub>-1.6</sub>	-0.78 ± 0.20	-0.88 ± 0.10	0.24 ± 0.18	-0.23 ± 0.20
VCC0725 <sup>a</sup>	5.5 <sup>+1.4</sup> <sub>-1.7</sub>	—	-1.00 ± 0.25	—	0.16 ± 0.38	—
VCC0856	1.9 <sup>+0.2</sup> <sub>-0.1</sub>	15.0 <sup>+0.0</sup> <sub>-5.1</sub>	0.03 ± 0.10	-0.61 ± 0.07	-0.14 ± 0.06	0.03 ± 0.16
VCC0929	3.2 <sup>+0.5</sup> <sub>-0.4</sub>	3.8 <sup>+1.4</sup> <sub>-0.6</sub>	0.11 ± 0.07	0.03 ± 0.10	-0.16 ± 0.05	0.15 ± 0.07
VCC0990	2.3 <sup>+0.9</sup> <sub>-0.4</sub>	5.5 <sup>+2.1</sup> <sub>-1.1</sub>	-0.19 ± 0.15	-0.31 ± 0.17	-0.30 ± 0.04	-0.01 ± 0.12
VCC1167	15 <sup>+0.0</sup> <sub>-0.0</sub>	7.5 <sup>+7.5</sup> <sub>-2.3</sub>	-1.15 ± 0.05	-0.65 ± 0.22	0.09 ± 0.16	0.09 ± 0.18
VCC1185	11.9 <sup>+0.6</sup> <sub>-2.4</sub>	12.5 <sup>+1.2</sup> <sub>-1.1</sub>	-1.37 ± 0.05	-0.68 ± 0.10	-0.22 ± 0.33	-0.01 ± 0.22
VCC1254	5.7 <sup>+1.2</sup> <sub>-1.2</sub>	15.0 <sup>+0.0</sup> <sub>-9.0</sub>	-0.43 ± 0.10	-0.48 ± 0.32	0.05 ± 0.07	-0.11 ± 0.14
VCC1261	1.8 <sup>+0.1</sup> <sub>-0.0</sub>	6.9 <sup>+2.2</sup> <sub>-1.4</sub>	0.18 ± 0.00	-0.46 ± 0.15	-0.10 ± 0.07	0.07 ± 0.12
VCC1304	8.6 <sup>+4.4</sup> <sub>-2.1</sub>	4.5 <sup>+0.7</sup> <sub>-2.0</sub>	-1.22 ± 0.20	-0.56 ± 0.27	-0.30 ± 0.10	-0.22 ± 0.19
VCC1308	1.8 <sup>+0.3</sup> <sub>-0.2</sub>	15.0 <sup>+0.0</sup> <sub>-10.2</sub>	+0.16 ± 0.12	-0.70 ± 0.42	0.09 ± 0.09	0.11 ± 0.18
VCC1333	7.9 <sup>+5.8</sup> <sub>-1.0</sub>	1.0 <sup>+0.4</sup> <sub>-0.0</sub>	-1.05 ± 0.20	-0.97 ± 0.20	0.07 ± 0.20	0.04 ± 0.37
VCC1348	10.9 <sup>+2.2</sup> <sub>-1.4</sub>	15.0 <sup>+0.0</sup> <sub>-1.3</sub>	-0.80 ± 0.10	-0.53 ± 0.07	0.45 ± 0.14	0.50 ± 0.04
VCC1353	3.2 <sup>+1.2</sup> <sub>-1.2</sub>	4.1 <sup>+1.6</sup> <sub>-1.4</sub>	-1.02 ± 0.25	-0.58 ± 0.22	-0.26 ± 0.32	0.38 ± 0.18
VCC1355	1.8 <sup>+2.3</sup> <sub>-0.5</sub>	3.2 <sup>+1.8</sup> <sub>-0.6</sub>	-0.48 ± 0.39	-0.34 ± 0.22	-0.08 ± 0.30	-0.04 ± 0.16
VCC1389	13.1 <sup>+1.9</sup> <sub>-3.1</sub>	11.9 <sup>+0.0</sup> <sub>-2.0</sub>	-1.27 ± 0.20	-0.85 ± 0.10	0.07 ± 0.30	0.19 ± 0.19
VCC1407	2.6 <sup>+1.3</sup> <sub>-0.7</sub>	14.3 <sup>+0.7</sup> <sub>-8.6</sub>	-0.12 ± 0.17	-0.73 ± 0.34	0.07 ± 0.14	0.11 ± 0.16
VCC1661	9.1 <sup>+5.9</sup> <sub>-1.5</sub>	6.6 <sup>+3.8</sup> <sub>-1.1</sub>	-0.95 ± 0.15	-0.36 ± 0.22	-0.26 ± 0.14	-0.30 ± 0.04
VCC1826	1.7 <sup>+0.6</sup> <sub>-0.2</sub>	11.4 <sup>+1.7</sup> <sub>-2.3</sub>	+0.13 ± 0.17	-0.90 ± 0.15	-0.07 ± 0.13	-0.10 ± 0.19
VCC1861	3.8 <sup>+2.2</sup> <sub>-1.0</sub>	4.1 <sup>+1.3</sup> <sub>-1.3</sub>	-0.29 ± 0.17	-0.12 ± 0.12	-0.16 ± 0.14	0.07 ± 0.09
VCC1945	6.6 <sup>+8.4</sup> <sub>-1.3</sub>	14.3 <sup>+0.7</sup> <sub>-2.4</sub>	-0.75 ± 0.27	-1.00 ± 0.10	0.00 ± 0.24	-0.30 ± 0.23
VCC2019	1.7 <sup>+0.2</sup> <sub>-0.3</sub>	8.3 <sup>+6.1</sup> <sub>-2.5</sub>	+0.06 ± 0.15	-0.41 ± 0.24	-0.27 ± 0.12	0.00 ± 0.16

<sup>a</sup>without subtraction of galactic light and does not have a measurement of SSPs from the galactic main body (see text).

In the right part of Figure 2, the green vertical bars present, for comparison, the derived stellar population parameters of the UCD sample of [Evstigneeva et al. \(2007\)](#). Note that we only use the published four indices ( $H\beta$ ,  $Mgb$ ,  $Fe5270$  and  $Fe5335$ ). However, we use the same method of estimation for the stellar population parameters. The UCD ages and metallicities are consistent with old and metal poor stellar populations. Almost all UCDs have ages  $\sim 10$  Gyr and metallicities vary between -1.25 to 0.13 dex. The [ $\alpha$ /Fe]-abundances are always super solar in case of the UCDs, with a mean of 0.31 dex, which is 0.34 dex higher than the mean [ $\alpha$ /Fe] of the dE nuclei.

The relation between the stellar population parameters and the local projected number density of galaxies in the cluster is plotted in Figure 3. The local projected density has been calculated from a circular projected area enclosing the 10th neighbor. It seems that there is a correlation between the local projected density and the ages of the nuclei. The Spearman rank order test shows a weak correlation of the ages and metallicities of the dE nuclei with the local projected densities. The correlation coefficients are 0.5 and -0.4, and the probabilities of the null hypothesis that there is no correlation are 0.2% and 4% for the age and metallicity, respectively. Unlike this, a similar test shows that the SSPs of the galactic main body do not have any relation with local projected densities.

The relations between the stellar population param-

eters and the total galactic luminosity are presented in Fig. 4. At the top of each panel, we also provide the trend of the differences in the SSP parameters between the galactic main bodies and the nuclei. It is clearly recognized that almost all dEs brighter than  $M_r = -17$  mag have younger and more metal-rich nuclei than the galactic main bodies. On the other hand, there is a relatively large scatter in the low luminosity region, and we can see that some of the nuclei are as old and metal poor as the galactic main bodies. However, the sign of the differences in age and metallicity between galactic main body and nucleus are completely opposite at the fainter and brighter end of the plot. As there exists a well-known metallicity-luminosity relation in early type galaxies ([Poggianti et al. 2001](#)), our sample also follows this relation for both nuclei and galaxies, i.e., the metallicity decreases with decreasing total galactic luminosity. The derived [ $\alpha$ /Fe] values are fairly consistent with a roughly solar value for both nuclei and galactic main bodies.

In the right panels of Fig. 4, we provide the number distribution (in the histogram) of stellar population parameters of the nuclei (in blue color) and the galactic main bodies (in green color). It seems that the ages of the galactic main bodies have a bimodal distribution, but the small number of data points in each bin and the fairly large errors in the age measurement increase the uncertainty; the bimodality thus remains a qualitative impression. The age distribution of the nuclei is highly dominated by nuclei of

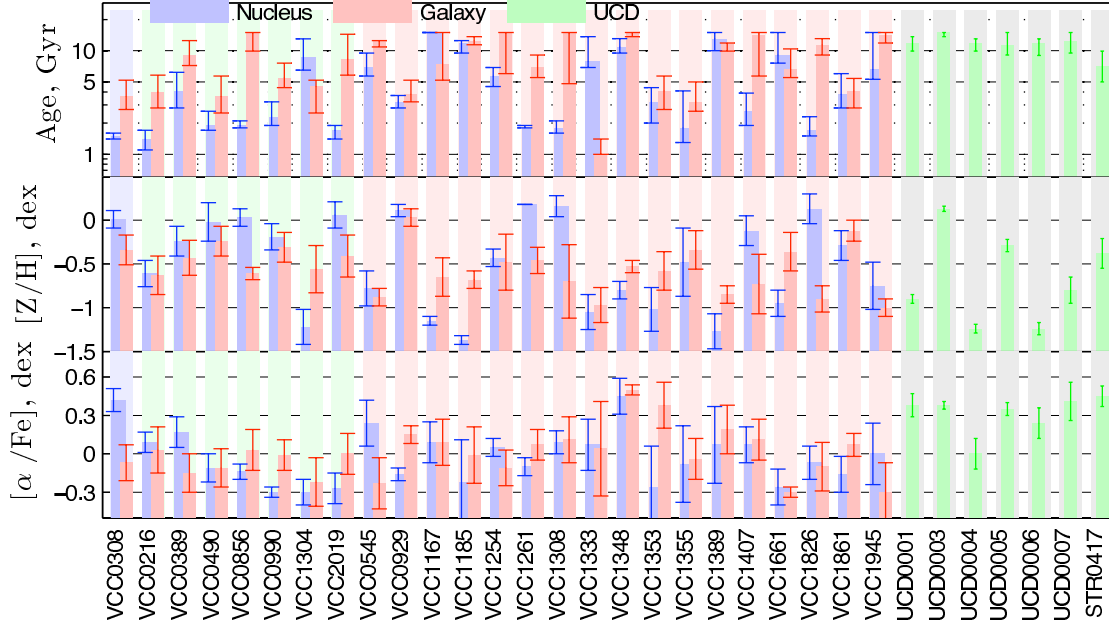


**Figure 2.** A comparison of stellar population parameters. The SSPs from the different parts of the dEs are represented with vertical bars of different color: blue for the nuclei and red for the galactic main bodies. The faint background colors indicate the dE subtype: blue for the nucleated dE with disk and blue centre, green for the nucleated dEs with disks, and red for the nucleated dEs without disk features. The Virgo UCDs are represented by the green vertical bars with gray background. For the UCDs, we used published values of line strengths from [Evstigneeva et al. \(2007\)](#) to derive the stellar population parameters (see text).

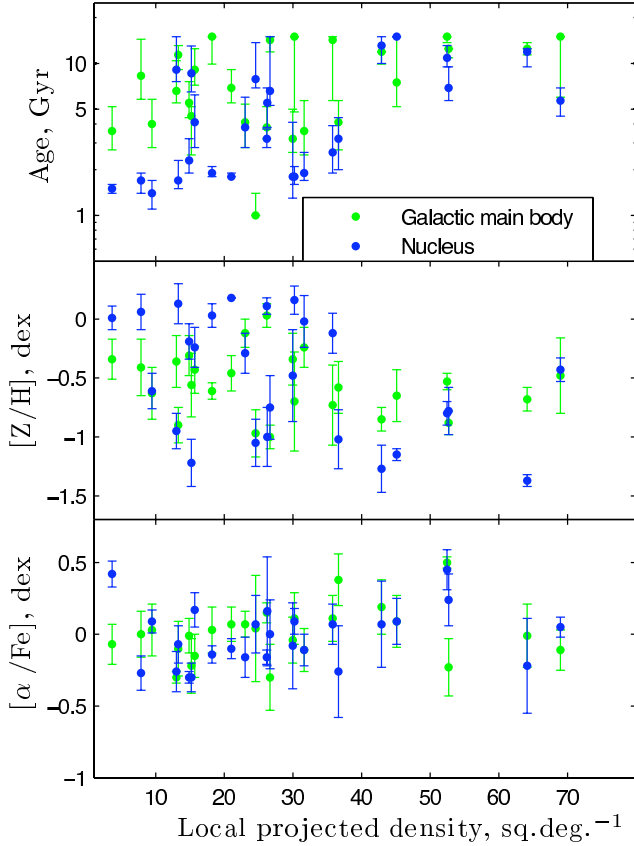


**Figure 3.** The age, metallicity and  $[\alpha/\text{Fe}]$  versus local projected density. Green color represents the galactic main body and blue indicates the nucleus.

younger ages. The metallicity distribution however appears much broader in case of nuclei than galactic main body. The nucleus metallicity ranges from slightly super-solar (+0.18 dex) to strongly sub-solar values (-1.22 dex), and interestingly all dE galactic main bodies have sub-solar metallicity.

#### 4.1 Stellar population gradients

Due to the low brightness of dEs, it is always challenging to get spectra from their outer part with sufficient SNR to study stellar population gradients. Some attempts have been made to derive the stellar population gradients in the different cluster dEs ([Chilingarian 2009](#) for Virgo, [Koleva et al. 2009](#) for Fornax). These studies used different methods to obtain SSP parameters, namely through spectral fitting with SSP models. [Chilingarian \(2009\)](#) observed either flat or negative radial gradients in metallicity in his sample. However, due to the relatively high uncertainty in the age estimation, he did not draw conclusions on the radial behavior of ages. The study of [Koleva et al. \(2009\)](#) reconfirmed the result of the existence of negative metallicity gradients and found radial age gradients in the dEs, with older ages at larger radii.

In Figure 5–8, we present the radial profiles of SSP-equivalent age, metallicity and abundance ratio, measured in bins along the major axis of the dEs. It is interesting that we can divide these trends of SSPs in two groups. The first group are those dEs which exhibit a smooth trend of increasing the age and decreasing metallicity with radius, beginning from the nucleus, such as VCC0308, VCC0490, VCC0929, VCC1261 and VCC2019. In contrast, the second group shows a break in the SSP profile when going from the nucleus to the surrounding galactic part, with the latter hav-

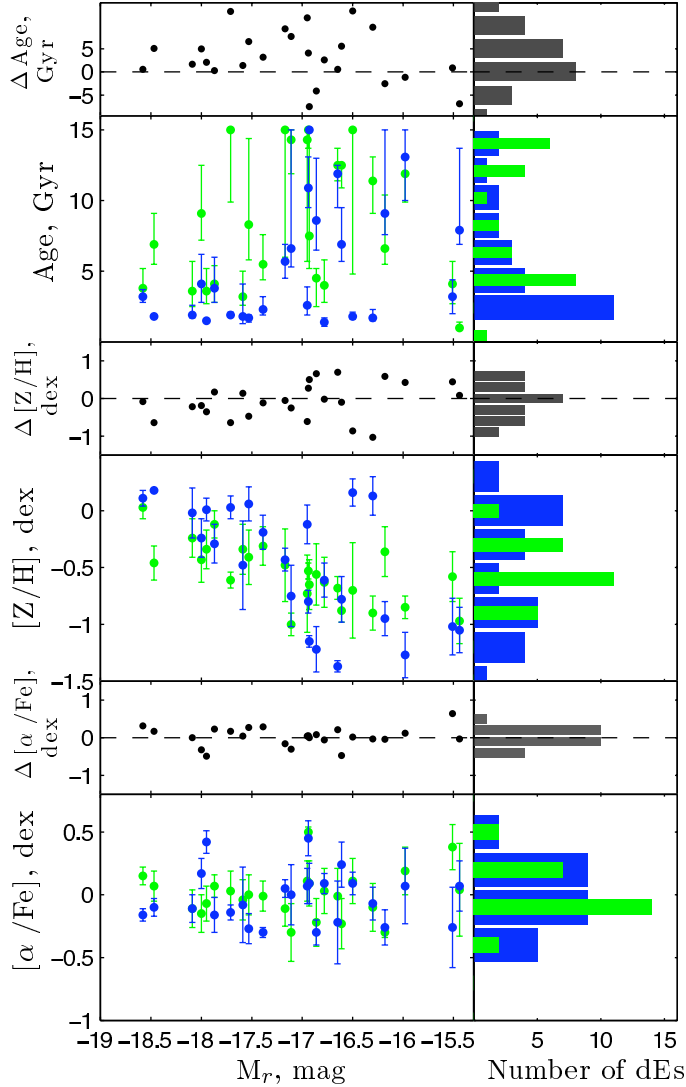


**Figure 4.** The derived ages (top), metallicities (middle) and  $[\alpha/\text{Fe}]$ -abundance (bottom), plotted against  $r$ -band absolute magnitude (left). The blue color represents the nuclei and green color indicates the galactic main body. On top of each panel, we also show the difference in the SSP parameters, i.e. galactic part – nucleus. In the right panel, we provide the number distribution of the parameters.

ing a nearly flat gradient, like e.g. for VCC0216, VCC0856, VCC1304 and VCC1355.

Three dEs, VCC2019, VCC1261 and VCC0308, show a significant gradient in age and metallicity, having a relatively young and metal enhanced nucleus. Likewise, the ages of VCC0389, VCC0490, VCC0990, VCC0929 and VCC1407 also seem to correlate with the radius. Our derived ages for VCC0856 agree with the result of Chilingarian (2009) that this galaxy has a flat distribution of ages beyond the central nucleus. In addition to that, we can also see such a flatness in the age distribution of VCC1355. VCC1261 presents the largest gradient in metallicity starting from slightly super solar down to a sub-solar value of  $-0.75$  dex. Although we do not see any strong trend of  $[\alpha/\text{Fe}]$  with radius in most of the cases, VCC0216 and VCC2019 display the opposite

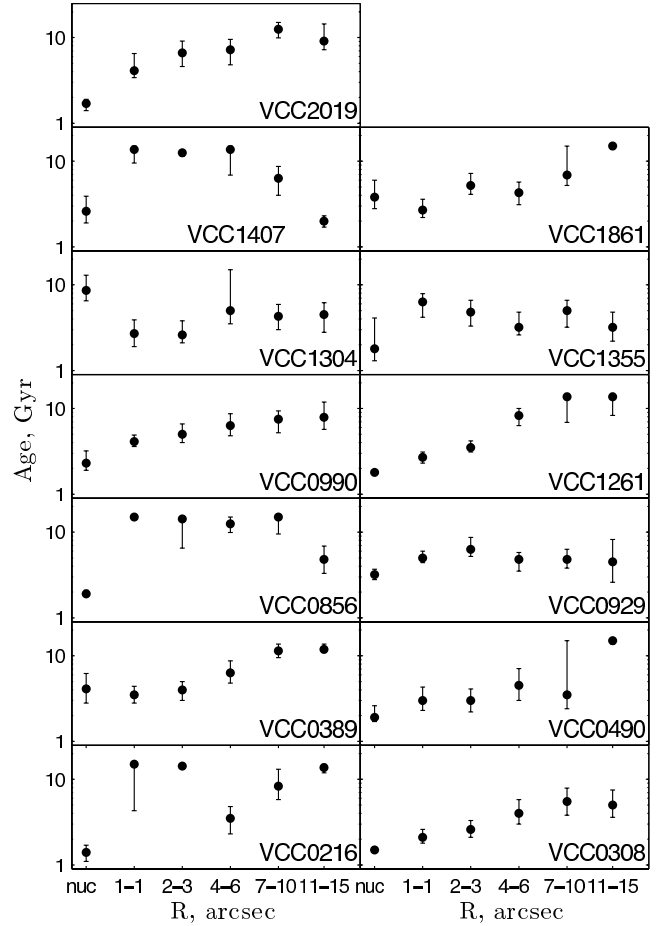


**Figure 5.** The radial age profiles of selected dEs (here we select those dEs which have sufficient SNR at the last radial bin,  $11''$  to  $15''$ ).

trend of decreasing and increasing of  $[\alpha/\text{Fe}]$  with radius, respectively.

In Figure 7 we show the age and metallicity distribution of our dEs in the different radial bins. Note that there is not always the same number of dEs in each radial bin: due to insufficient SNR in the outer radii for some dEs, those were omitted from the respective bins. The first  $1''$  bin contains 25 dEs, and the second, third and fourth bin contains 24, 20 and 16 dEs, respectively. Therefore, the y-axis represents the normalized fraction in percent. It is easily noticeable that the distributions change with radius: the inner bin is dominated by young ages and shows a broader metallicity distribution, and the fraction of old ages and low metallicities increases as we go outward, with the metallicity distribution becoming narrower.

## 5 DISCUSSION

In this paper, we have characterized the stellar population parameters from the different parts of dEs: the nuclei and the surrounding galactic main bodies. Our primary motivation for this is to improve our understanding of the physical mechanisms responsible for the formation of dE nuclei and the subsequent evolution of dEs themselves. As we now



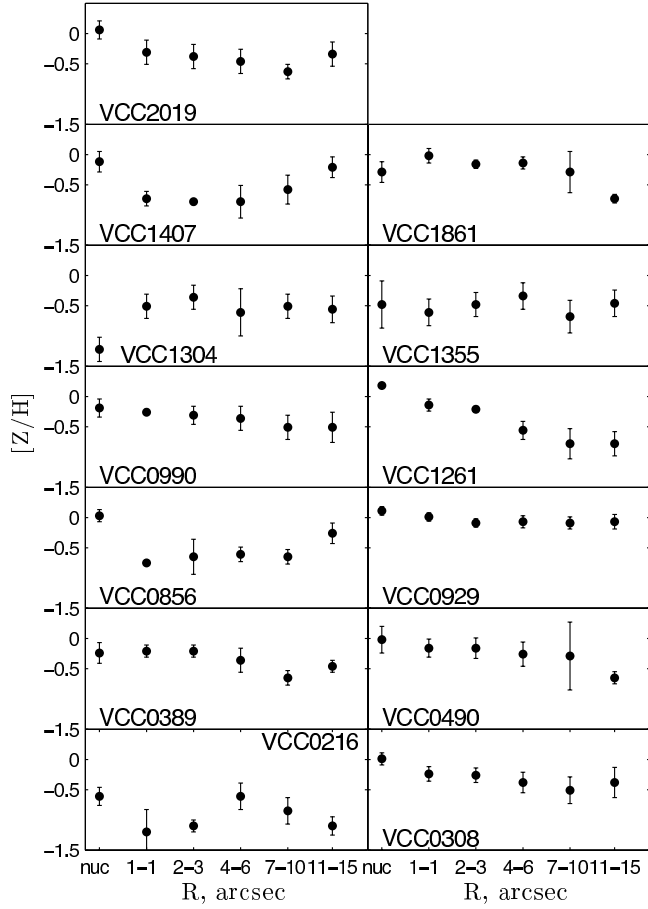


**Figure 6.** The radial metallicity profiles of the dEs, selected as in Fig. 5.

discuss, our study makes two important contributions in this context: (i) to much more firmly establish the SSP-equivalent stellar population parameters of dEs and their nuclei (ii) to cast new light on the spatially resolved stellar population characteristics of dEs.

The surrounding galactic main body is represented by extracting its spectrum from a 5'' radial interval beyond 3'' from the centre, avoiding any contamination with light from the nucleus. We expect that, due to our method of subtraction of the underlying galactic light from the nucleus spectra (see Appendix A), we obtained comparatively clean spectra of the nuclei, with the derived stellar population properties from such spectra well representing the nucleus stellar population. Nevertheless, as outlined before, in the cases of weak nuclei there is still a chance that the remaining galactic light contributes significantly, such that the nuclear spectra represent the combination of nucleus and “central galaxy light”. To test for a possible bias due to this effect, we select those dEs which have galactic light fraction (see Table 1) larger than 50% at the central aperture such as VCC0990, VCC1353, VCC1355, VCC1407 and VCC1826, but all these nuclei have ages less than 5 Gyr, and agree fairly well with the average age of the nuclei in total.

Generally speaking, stellar population gradients can be used as a proxy for the study of the evolutionary history of early type galaxies, since different formation models predict

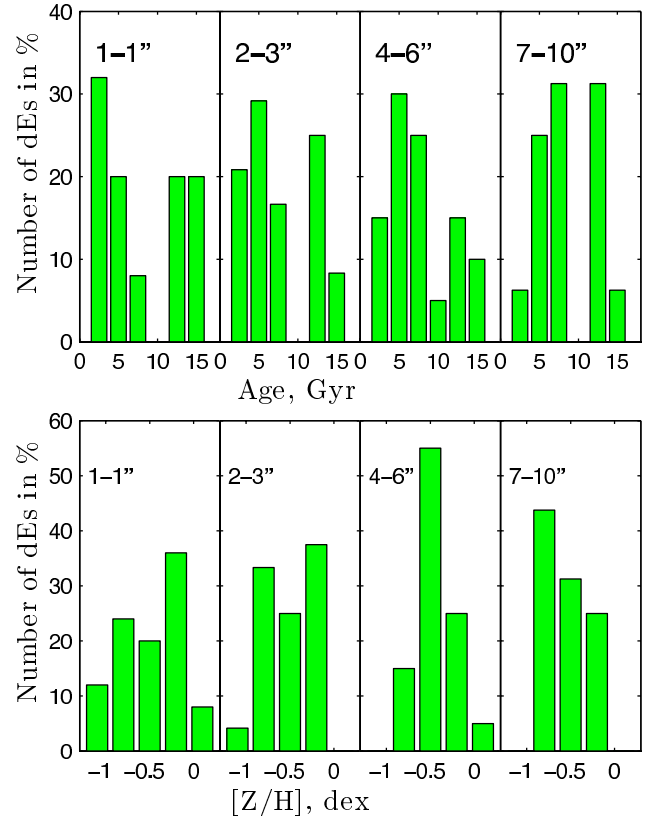


**Figure 7.** The age and metallicity distribution at different radial bins.

different gradients. In a nutshell, monolithic collapse models (Arimoto & Yoshii 1987) predict slightly steeper gradients than the hierarchical merging model (White 1980). These predictions, however, mainly apply to normal early-type galaxies (Es). In case of early-type dwarfs, different formation scenarios might be relevant, such as morphological transformation, or simply a primordial origin (also see the discussion in Paper I). Nevertheless, the overall distribution of age and metallicity at the different radial bins suggest that it occurs more frequently that the inner parts of dEs are younger and more metal enhanced than their outer parts, which is consistent with previous studies (Chilingarian 2009; Koleva et al. 2009). We also see two distinct behaviours of radial SSP profiles; the presence of flat profiles may be due to a particular galaxy structure (i.e., a faint underlying disk) or may be an indication of a different origin. Among the dEs with smooth SSP gradients, VCC0308 only has a very weak blue centre (Lisker et al. 2006), so it may well be that other galaxies have just a bit weaker colour gradients and were thus not labeled “blue-centre dE” previously. On the other hand, VCC0216 and VCC0856 have a similarly young nucleus as VCC0308, but not an age gradient in the galaxy itself, which might lead to having no colour gradient.

Another key result emerging from our study is a very clear picture of the differences between the stellar populations of the nuclei and the galactic main bodies of the dEs. To our knowledge, no spectroscopic study has yet performed such a comparison with a similar sample size. Studies based on color differences (Durrell 1997; Côté et al. 2006, and particularly Lotz et al. 2004) find slightly bluer nuclei.

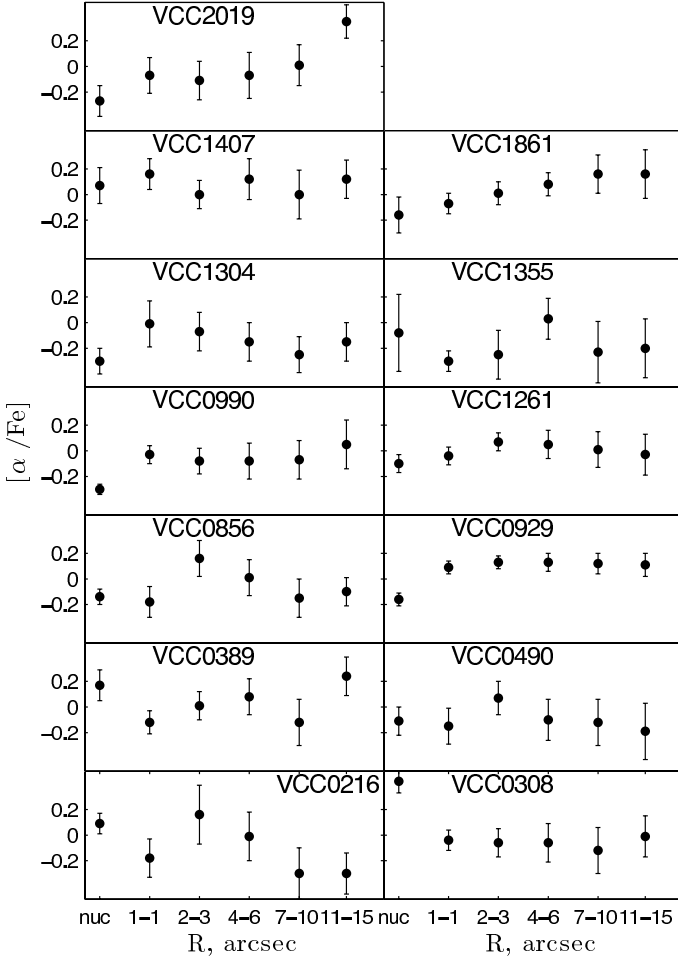


**Figure 8.** The radial profile of the  $\alpha$ -abundance ratios of the dEs, selected as in Fig. 5.

It is, however, not straightforward to interpret these color differences in the sense of stellar population properties, as we know that a degeneracy in the age and metallicity exists with color (see also Appendix B). In contrast to the explanation of Lotz et al. (2004) of having more metal rich populations in the surrounding galactic main bodies, we find a metal poorer and older population in the galactic part on average. In addition to this, as Côté et al. (2006) note, there exists a color-luminosity relation for the nuclei. We also find that the metallicity of dE nuclei correlates with the total luminosity of dEs.

We have seen that there is almost no correlation between the ages of the galactic main bodies and the luminosity of the dEs. This might, at first glance, imply that the reason for the apparent age dichotomy in Paper I, finding a clear correlation with luminosity for the central stellar populations of dEs, was due to the nucleus contribution to the central aperture light. However, Fig. A2 of the Appendix, which compares the SSPs resulting from the nucleus spectra before and after subtraction of the underlying galactic light, actually tells us that this conclusion is not true: if the very central stellar populations of the galaxies, whose pure light cannot be seen due to the superposed nucleus, would be so much older than the nucleus itself, the difference be-

fore/after subtraction would be quite significant, which is not found. Instead, the figure tells us that the very central part of the galaxy does also reach, in most cases, almost the young age of the nuclei. Thus, in many cases it is really the age gradient within the galaxy that makes the galactic part surrounding the nucleus appear significantly older than the nucleus itself in Fig. 4.

### 5.1 Evolution of dEs and formation of nuclei

As we mentioned in the introduction, many studies have discussed the origin of the nuclei of dEs together with the evolution of dEs themselves. It is challenging to provide definitive observational tests of these different scenarios. Moreover, we argue in Paper I that not all dEs are the same class of object. The dichotomy in the age distribution of the galactic main bodies also supports the idea that one type of dEs may have a primordial origin (Rakos & Schombert 2004), being relatively old and metal poor. These might have suffered either early infall into the cluster potential or formed together with the cluster itself. The common idea is that internal feedback might be responsible for the removal of gas, with the consequence that star formation activity ceases at such early epochs.

On the other hand, dEs with a relatively young and metal enhanced galactic main body likely have a different origin. As they are also preferentially brighter and often host disk-structure, they might have formed through the structural transformation of a late-type spiral into a spheroidal system, triggered by the popular scenario of strong tidal interactions with massive cluster galaxies. Simulations have shown that late-type galaxies entering in a rich cluster can undergo a significant morphological transformation into spheroidals by encounters with brighter galaxies and with the cluster's tidal field (Moore et al. 1996; Mastropietro et al. 2005). This scenario is unlikely to produce the observed radial SSP gradients: either metallicity gradients must have formed in the late-type galaxies and somehow preserved during morphological transformation (see the discussion in Spolaor et al. 2010), or accretion of leftover gas towards the centre of the galaxy would have to be responsible for the creation of such gradients. However, the flat  $[\alpha/\text{Fe}]$  profile implies a similar star formation time scale everywhere in the dEs.

As we discussed above, the fairly different types of dEs with and without disk structure might have a different origin. It is therefore even more difficult to explain the origin of the nuclei of these dEs with a single scenario. However, from this and previous studies, it is becoming clear that the majority of dE nuclei are unlikely to have formed through the merging of globular clusters: Côté et al. (2006) already explained the difficulty of this scenario with the luminosity differences, and additionally we find that most nuclei are fairly young and metal rich, at least in case of the brighter dEs ( $M_r \leq -17.25$  mag). There are still the nuclei of some fainter dEs (i.e.,  $M_r > -17.25$  mag) which have fairly old and metal-poor populations, more resembling the stellar population properties of globular clusters. They might have formed through a different process as the nuclei of brighter dEs.

The younger and comparably metal-rich nuclei support the idea that the central stellar populations of dEs were gov-

erned by continuous infall and accretion of gas in the centre of the potential well, building the nuclei. The brighter dEs also host disk features (e.g. residual spiral arms/bars) and these dEs themselves might have been formed through the transformation of late-type spirals (Sc-Sd types). High resolution HST imaging has shown that such late-type objects frequently contain a compact nuclear cluster (Böker et al. 2002, 2004), and Côté et al. (2006) observed that such nuclear clusters have similar sizes to dE nuclei. Stellar population studies have shown that the majority of nuclear clusters have ages of few tens of Myr (Seth et al. 2006; Walcher et al. 2006) with episodic star formation activity. Following the simplest interpretation, it could be that the present day dE nuclei are simply the nuclear clusters of the transformed late-type galaxies, and their star formation activity faded with the morphological transformation of the host galaxies. However, this scenario again fails to explain the observed age difference between the nuclei and galactic main bodies, since late type disks are also considered to host star formation activity throughout the inner region and disk. Alternatively, the truncation of star formation in the disk due to interactions could be more efficient than in the nucleus, which eventually leads to the development of age/metallicity gradients in dEs and makes the central nucleus younger and metal richer than the galactic main body. In any case, more detailed numerical simulations are required to test these hypotheses.

We find that dE nuclei exhibit fairly different stellar populations than UCDs. Particularly, the relatively older population (larger than 8 Gyr) and slightly super-solar  $\alpha$ -abundance of UCDs may seem to create an inconsistency in the idea of dE nuclei being the progenitors of UCDs. Nevertheless, the current sample of UCDs is limited, and the fairly large spread in the stellar population properties of dE nuclei may allow the possibility of UCD formation in the Virgo cluster by the stripping of such dEs whose nuclei have old and metal poor stellar populations (Paudel et al. 2010). Therefore, a larger sample of UCDs and perhaps a more rigorous comparison of SSP properties than this work is needed before any strong conclusions can be drawn.

## 6 CONCLUSIONS

We have investigated the stellar population properties of the central nucleus and the surrounding galactic main body for a sample of 26 dEs in the Virgo cluster and compared the SSP-equivalent stellar population parameters of the dE nuclei with the ones of a small sample of UCDs. In addition to this, we have derived the radial profiles for age, metallicity and  $[\alpha/\text{Fe}]$  abundance for 13 dEs. Our main findings can be summarized as follows:

- We find that for most of the dEs the nuclei are significantly younger ( $\sim 3.5$  Gyr) and more metal rich ( $\sim 0.07$  dex) as compared to the galactic main body of the galaxies. Only five dEs have significantly older nuclei than their galactic main bodies, and dEs with old and metal poor nuclei are more likely to be distributed in the dense region of the cluster than the dEs with young and metal-enhanced nuclei.
- The metallicity of dE nuclei correlates with the total luminosity of dEs, and the observed metallicities of the nuclei

have a fairly large range (+0.18 to -1.22 dex). All galactic main bodies of the dEs have sub-solar metallicity.

- While we see two distinct behaviours of SSP profiles (with and without a break) the overall trend of increasing age and decreasing metallicity with the radius is consistent with earlier studies. The  $\alpha$ -abundance as function of radius is consistent with no gradient.

- These observed properties suggest that the merging of globular clusters might not be the appropriate scenario for the formation of nuclei in dEs, at least not for the brighter dEs. The younger and comparably metal-rich nuclei support the idea that the central stellar populations of dEs were governed by continuous infall/accretion of gas in the centre of the potential well, building the nuclei.

- The heterogeneous nature of the stellar population characteristics of dEs hints at different formation scenarios of dEs, similar to the conclusion of our previous study (Paudel et al. 2010). Our results suggest that the old, faint and metal-poor dEs are more likely to have a primordial origin, while those with relatively young ages and a higher metallicity and luminosity may have formed through morphological transformation.

## 7 ACKNOWLEDGMENTS

We thank Michael Hilker for useful comments. We thank the referee for providing useful suggestions for improving the manuscript. S.P. and T.L. are supported within the framework of the Excellence Initiative by the German Research Foundation (DFG) through the Heidelberg Graduate School of Fundamental Physics (grant number GSC 129/1). S.P. acknowledges the support of the International Max Planck Research School (IMPRS) for Astronomy and Cosmic Physics at the University of Heidelberg. This work was based on observations made with ESO telescopes at Paranal Observatory under programme ID 078.B-0178(A). This work has made use of the NASA Astrophysics Data System and the NASA/IPAC Extragalactic Data base (NED) which is operated by the Jet Propulsion Laboratory, California Institute of Technology, under contract with the National Aeronautics and Space Administration.

## REFERENCES

- Arimoto N., Yoshii Y., 1987, *A&A*, 173, 23
- Babul A., Rees M. J., 1992, *MNRAS*, 255, 346
- Bekki K., Couch W. J., Drinkwater M. J., Shioya Y., 2003, *MNRAS*, 344, 399
- Binggeli B., Cameron L. M., 1991, *A&A*, 252, 27
- Binggeli B., Cameron L. M., 1993, *A&AS*, 98, 297
- Binggeli B., Sandage A., Tammann G. A., 1985, *AJ*, 90, 1681
- Binggeli B., Tammann G. A., Sandage A., 1987, *AJ*, 94, 251
- Böker T., Laine S., van der Marel R. P., Sarzi M., Rix H., Ho L. C., Shields J. C., 2002, *AJ*, 123, 1389
- Böker T., Sarzi M., McLaughlin D. E., van der Marel R. P., Rix H., Ho L. C., Shields J. C., 2004, *AJ*, 127, 105
- Burstein D., Faber S. M., Gaskell C. M., Krumm N., 1984, *ApJ*, 287, 586
- Caldwell N., Rose J. A., Concannon K. D., 2003, *AJ*, 125, 2891
- Chilingarian I. V., 2009, *MNRAS*, 394, 1229
- Côté P., Piatek S., Ferrarese L., Jordán A., Merritt D., Peng E. W., Hasegan M., Blakeslee J. P., Mei S., West M. J., Milosavljević M., Tonry J. L., 2006, *ApJS*, 165, 57
- Drinkwater M. J., Gregg M. D., Hilker M., Bekki K., Couch W. J., Ferguson H. C., Jones J. B., Phillipps S., 2003, *Nature*, 423, 519
- Durrell P. R., 1997, *AJ*, 113, 531
- Evstigneeva E. A., Gregg M. D., Drinkwater M. J., Hilker M., 2007, *AJ*, 133, 1722
- Ferguson H. C., Binggeli B., 1994, *A&AR*, 6, 67
- Ferguson H. C., Sandage A., 1989, *ApJ*, 346, L53
- Geha M., Guhathakurta P., van der Marel R. P., 2003, *AJ*, 126, 1794
- Goerdt T., Moore B., Kazantzidis S., Kaufmann T., Macciò A. V., Stadel J., 2008, *MNRAS*, 385, 2136
- Graham A. W., Guzmán R., 2003, *AJ*, 125, 2936
- Grant N. I., Kuipers J. A., Phillipps S., 2005, *MNRAS*, 363, 1019
- Hilker M., Infante L., Vieira G., Kissler-Patig M., Richtler T., 1999, *A&AS*, 134, 75
- Janz J., Lisker T., 2008, *ApJ*, 689, L25
- Koleva M., de Rijcke S., Prugniel P., Zeilinger W. W., Michielsen D., 2009, *MNRAS*, 396, 2133
- Lisker T., Glatt K., Westera P., Grebel E. K., 2006, *AJ*, 132, 2432
- Lisker T., Grebel E. K., Binggeli B., 2006, *AJ*, 132, 497
- Lisker T., Grebel E. K., Binggeli B., 2008, *AJ*, 135, 380
- Lisker T., Grebel E. K., Binggeli B., Glatt K., 2007, *ApJ*, 660, 1186
- Lotz J. M., Miller B. W., Ferguson H. C., 2004, *ApJ*, 613, 262
- Mastropietro C., Moore B., Mayer L., Debattista V. P., Piffaretti R., Stadel J., 2005, *MNRAS*, 364, 607
- Mei S., Blakeslee J. P., Côté P., Tonry J. L., West M. J., Ferrarese L., Jordán A., Peng E. W., Anthony A., Merritt D., 2007, *ApJ*, 655, 144
- Michielsen D., Boselli A., Conselice C. J., Toloba E., Whiley I. M., Aragón-Salamanca A., Balcells M., Cardiel N., Cenarro A. J., Gorgas J., Peletier R. F., Vazdekis A., 2008, *MNRAS*, 385, 1374
- Moore B., Katz N., Lake G., Dressler A., Oemler A., 1996, *Nature*, 379, 613
- Oh K. S., Lin D. N. C., 2000, *ApJ*, 543, 620
- Paudel S., Lisker T., Janz J., 2010, in press (arXiv:1010.1076v1)
- Paudel S., Lisker T., Kuntschner H., Grebel E. K., Glatt K., 2010, *MNRAS*, 405, 800
- Phillipps S., Drinkwater M. J., Gregg M. D., Jones J. B., 2001, *ApJ*, 560, 201
- Poggianti B. M., Bridges T. J., Mobasher B., Carter D., Doi M., Iye M., Kashikawa N., Komiyama Y., Okamura S., Sekiguchi M., Shimasaku K., Yagi M., Yasuda N., 2001, *ApJ*, 562, 689
- Press W. H., Teukolsky S. A., Vetterling W. T., Flannery B. P., 1992, *Numerical recipes in C. The art of scientific computing*
- Proctor R. N., Sansom A. E., 2002, *MNRAS*, 333, 517
- Rakos K., Schombert J., 2004, *AJ*, 127, 1502
- Rakos K., Schombert J., Maitzen H. M., Prugovecki S., Odell A., 2001, *AJ*, 121, 1974
- Sandage A., Binggeli B., Tammann G. A., 1985, *AJ*, 90, 1759
- Seth A. C., Dalcanton J. J., Hodge P. W., Debattista V. P., 2006, *AJ*, 132, 2539
- Silk J., Wyse R. F. G., Shields G. A., 1987, *ApJ*, 322, L59
- Spolaor M., Hau G. K. T., Forbes D. A., Couch W. J., 2010, *ArXiv e-prints*
- Thomas D., Maraston C., Bender R., 2003, *MNRAS*, 339, 897
- Trager S. C., Faber S. M., Dressler A., 2008, *MNRAS*, 386, 715
- Trager S. C., Worthey G., Faber S. M., Burstein D., Gonzalez J. J., 1998, *ApJS*, 116, 1
- van den Bergh S., 1986, *AJ*, 91, 271
- van Zee L., Skillman E. D., Haynes M. P., 2004, *AJ*, 128, 121
- Vazdekis A., Sánchez-Blázquez P., Falcón-Barroso J., Cenarro A. J., Beasley M. A., Cardiel N., Gorgas J., Peletier R. F., 2010, *MNRAS*, 404, 1639
- Walcher C. J., Böker T., Charlot S., Ho L. C., Rix H., Rossa J., Shields J. C., van der Marel R. P., 2006, *ApJ*, 649, 692
- White S. D. M., 1980, *MNRAS*, 191, 1P
- Worthey G., Faber S. M., Gonzalez J. J., Burstein D., 1994, *ApJS*, 94, 687

## APPENDIX A: SUBTRACTION OF GALACTIC LIGHT FROM THE NUCLEUS

The Figure A1 provides a schematic view of the subtraction of galactic light from the central nucleus. First, we average the galaxy frame in the wavelength direction between 4000 Å to 5500 Å, assuming that there is not any severe change in light profile from exponential with the wavelength. The fitting of the galaxy light profile with an exponential has been done only considering the galaxy light beyond the 3" from the centre, because we assume that the light from the nucleus should not be spread out to these distances, as the mean FWHM is 1.25" for our observations.

The scaling of the galactic light to match the centre of the galaxy has been done by extrapolation of the light profile

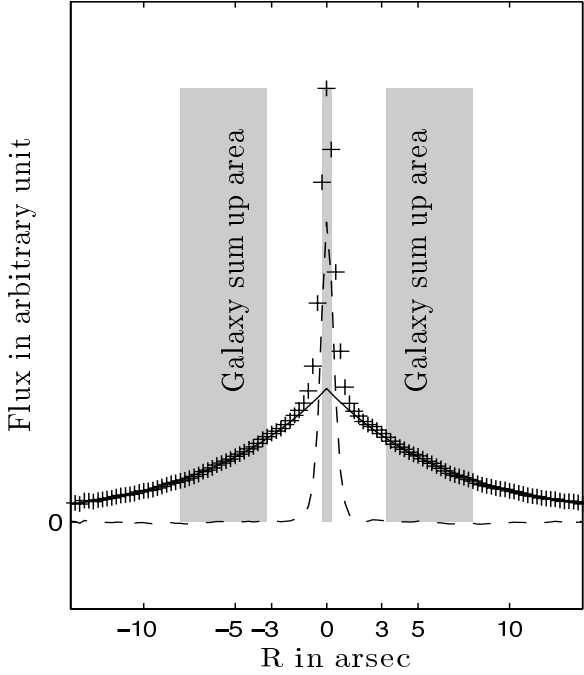


**Figure A1.** A schematic view of the fitting of the light profile for VCC0490 and the binning processes. The cross symbol represents the distribution of the observed total light (i.e galaxy + nucleus) and solid line represents the exponentially fitted light profile of the galaxy. The dashed line is the residual nucleus after the subtraction of galaxy light, which represents the pure nuclear light profile.

to the centre of dEs. The scale factor  $C$  has been calculated using the following equation,

$$C = \frac{\sum_{i=-1}^1 F_i^g}{\sum_{i=13}^{32} F_i^g} \quad (\text{A1})$$

where  $F^g$  is the flux from the best fitted galaxy profile (solid line in Fig. A1), and  $i$  is in pixel scale (i.e.,  $0.25''$ ) with the origin at the central peak of the observed slit profile of the galaxies. Then we subtract the galaxy light from the nucleus using

$$F_{\lambda}^{nuc} = \sum_{i=-1}^1 F_{\lambda i}^o - C \sum_{i=13}^{32} F_{\lambda i}^o \quad (\text{A2})$$

here,  $F^o$  is the observed light in the frame.

Although our exponential profiles of the galaxies are in good agreement with the observed profiles (see Fig. 1), some dEs have steeper profiles than exponential (Janz & Lisker 2008) - VCC0389, VCC0929, VCC1167, VCC1254, VCC1348 and VCC1861 have  $n \approx 2$ . Note, however, this finding is based on fitting a much larger radial interval from the imaging data. In these cases, we again derived the galactic light profile for  $n = 2$ , which produced a better match for VCC0929. However, the calculated difference of the amount of galaxy light which might be left at the centre when using  $n = 1$  was less than 30% of the total central light when compared to  $n = 2$ . Therefore, we always

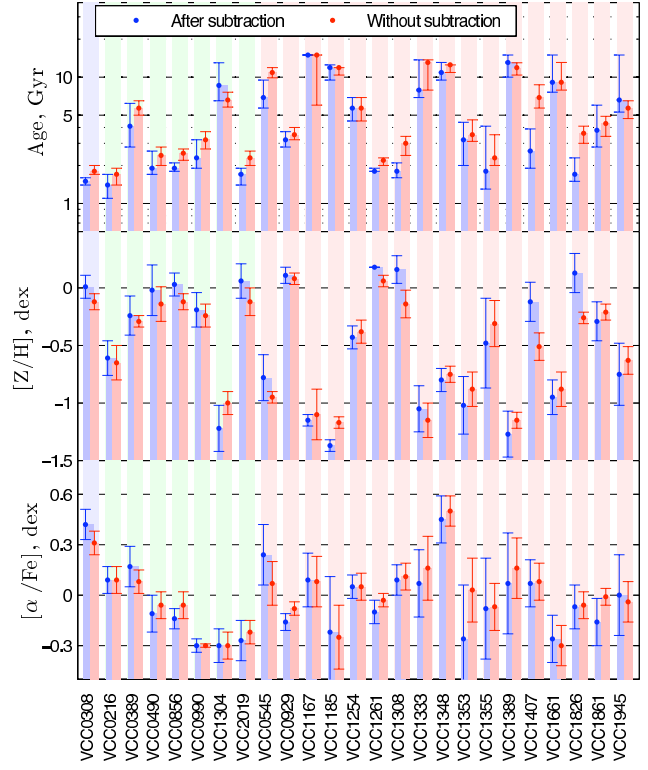


**Figure A2.** The comparison of the SSP-equivalent parameters after and before subtraction of galaxies' light from the nuclei spectra.

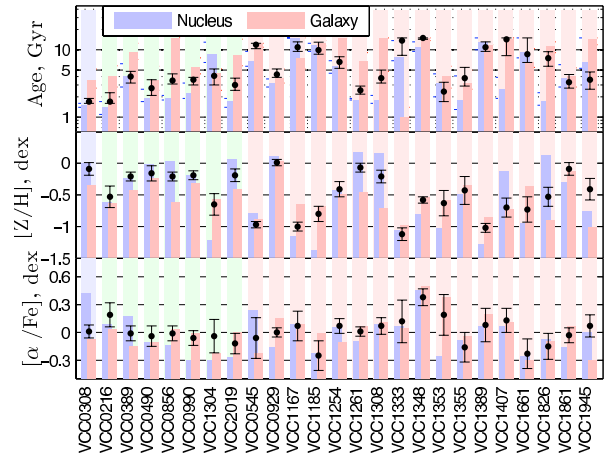


**Figure A3.** The comparison of the SSP-equivalent parameters of the galactic main bodies (red), nuclei of dEs (blue), and the result for the combined central light from Paper I (black), where a central spectrum was analysed without separating nucleus and galactic main body.

used the exponential profile for scaling the galactic light to the centre for all dEs.



**Table A1.** Measured line strength indices from the nuclei of dEs after subtraction of galactic light and corrected to the Lick system.

VCC no.	$H\delta_F$ Å	$H\gamma_F$ Å	Fe4383 Å	$H\beta$ Å	Fe5015 Å	$Mg_b$ Å	Fe5270 Å	Fe5335 Å	Fe5406 Å
0216	$4.75 \pm 0.27$	$3.78 \pm 0.24$	$0.06 \pm 0.64$	$3.11 \pm 0.28$	$3.82 \pm 0.62$	$1.28 \pm 0.31$	$1.69 \pm 0.35$	$0.68 \pm 0.39$	$1.44 \pm 0.28$
0308	$2.95 \pm 0.43$	$2.48 \pm 0.35$	$4.08 \pm 0.82$	$3.31 \pm 0.36$	$4.49 \pm 0.80$	$3.06 \pm 0.38$	$0.84 \pm 0.45$	$0.82 \pm 0.53$	$0.72 \pm 0.37$
0389	$2.78 \pm 0.50$	$-0.20 \pm 0.44$	$4.91 \pm 0.91$	$2.39 \pm 0.42$	$4.71 \pm 0.90$	$2.41 \pm 0.43$	$1.84 \pm 0.48$	$2.00 \pm 0.53$	$0.73 \pm 0.42$
0490	$1.87 \pm 0.47$	$0.94 \pm 0.40$	$4.04 \pm 0.87$	$2.89 \pm 0.38$	$4.59 \pm 0.83$	$2.17 \pm 0.41$	$2.71 \pm 0.45$	$2.10 \pm 0.51$	$1.24 \pm 0.37$
0545	$2.10 \pm 0.44$	$0.79 \pm 0.37$	$2.77 \pm 0.86$	$2.84 \pm 0.37$	$2.16 \pm 0.85$	$2.00 \pm 0.40$	$1.36 \pm 0.45$	$1.00 \pm 0.51$	$1.21 \pm 0.38$
0725 <sup>a</sup>	$2.01 \pm 0.57$	$2.28 \pm 0.50$	$2.16 \pm 1.22$	$3.55 \pm 0.52$	$2.55 \pm 1.24$	$1.44 \pm 0.57$	$1.16 \pm 0.67$	$0.54 \pm 0.77$	$0.39 \pm 0.56$
0856	$1.76 \pm 0.27$	$1.27 \pm 0.22$	$4.81 \pm 0.49$	$2.02 \pm 0.23$	$5.17 \pm 0.48$	$2.35 \pm 0.24$	$2.69 \pm 0.26$	$2.29 \pm 0.29$	$1.40 \pm 0.22$
0929	$0.04 \pm 0.31$	$-0.28 \pm 0.25$	$5.45 \pm 0.51$	$2.35 \pm 0.24$	$5.68 \pm 0.50$	$2.82 \pm 0.25$	$2.41 \pm 0.28$	$3.15 \pm 0.29$	$1.83 \pm 0.22$
0990	$1.02 \pm 0.59$	$1.01 \pm 0.45$	$3.03 \pm 0.97$	$2.94 \pm 0.39$	$5.80 \pm 0.82$	$1.33 \pm 0.41$	$2.71 \pm 0.44$	$1.25 \pm 0.51$	$2.35 \pm 0.36$
1167	$3.05 \pm 0.30$	$1.45 \pm 0.28$	$1.55 \pm 0.62$	$2.58 \pm 0.27$	$3.56 \pm 0.61$	$1.38 \pm 0.30$	$1.50 \pm 0.33$	$1.13 \pm 0.38$	$0.71 \pm 0.28$
1185	$1.37 \pm 0.44$	$2.05 \pm 0.34$	$2.03 \pm 0.85$	$2.17 \pm 0.41$	$2.36 \pm 0.90$	$1.04 \pm 0.43$	$1.08 \pm 0.48$	$0.48 \pm 0.54$	$0.44 \pm 0.41$
1254	$1.60 \pm 0.23$	$0.60 \pm 0.20$	$3.36 \pm 0.43$	$1.93 \pm 0.19$	$4.14 \pm 0.42$	$2.31 \pm 0.20$	$1.85 \pm 0.23$	$2.06 \pm 0.25$	$1.28 \pm 0.19$
1261	$1.58 \pm 0.32$	$0.45 \pm 0.27$	$4.07 \pm 0.59$	$2.77 \pm 0.26$	$6.05 \pm 0.55$	$2.76 \pm 0.27$	$3.27 \pm 0.30$	$2.95 \pm 0.34$	$1.42 \pm 0.25$
1304	$1.94 \pm 0.41$	$1.75 \pm 0.35$	$1.41 \pm 0.85$	$2.46 \pm 0.37$	$2.48 \pm 0.85$	$0.82 \pm 0.42$	$1.70 \pm 0.45$	$1.57 \pm 0.50$	$0.70 \pm 0.39$
1308	$1.39 \pm 0.58$	$1.28 \pm 0.46$	$5.30 \pm 1.00$	$2.55 \pm 0.45$	$1.11 \pm 1.10$	$3.11 \pm 0.47$	$1.44 \pm 0.55$	$2.24 \pm 0.61$	$1.52 \pm 0.46$
1333	$1.99 \pm 0.34$	$1.72 \pm 0.29$	$3.00 \pm 0.70$	$2.20 \pm 0.31$	$3.48 \pm 0.69$	$1.61 \pm 0.34$	$0.81 \pm 0.38$	$0.99 \pm 0.43$	$0.54 \pm 0.32$
1348	$1.68 \pm 0.36$	$0.29 \pm 0.32$	$2.40 \pm 0.69$	$2.16 \pm 0.31$	$3.07 \pm 0.68$	$2.26 \pm 0.32$	$1.74 \pm 0.36$	$0.85 \pm 0.42$	$0.50 \pm 0.31$
1353	$3.84 \pm 0.47$	$3.50 \pm 0.44$	$1.32 \pm 1.10$	$3.00 \pm 0.48$	$3.71 \pm 1.06$	$1.13 \pm 0.52$	$0.59 \pm 0.60$	$1.62 \pm 0.65$	$0.87 \pm 0.51$
1355	$4.12 \pm 0.75$	$1.72 \pm 0.76$	$2.67 \pm 1.76$	$2.75 \pm 0.76$	$2.89 \pm 1.74$	$1.44 \pm 0.80$	$2.42 \pm 0.89$	$1.66 \pm 1.02$	$1.42 \pm 0.75$
1389	$3.15 \pm 0.47$	$1.27 \pm 0.44$	$1.47 \pm 1.01$	$1.65 \pm 0.44$	$2.75 \pm 0.98$	$1.37 \pm 0.46$	$0.72 \pm 0.52$	$1.33 \pm 0.58$	$0.97 \pm 0.42$
1407	$1.61 \pm 0.70$	$0.69 \pm 0.54$	$2.96 \pm 1.25$	$2.52 \pm 0.50$	$4.47 \pm 1.05$	$2.64 \pm 0.50$	$1.43 \pm 0.57$	$2.42 \pm 0.61$	$1.92 \pm 0.46$
1661	$2.11 \pm 0.41$	$0.35 \pm 0.36$	$3.02 \pm 0.82$	$2.49 \pm 0.36$	$3.33 \pm 0.82$	$1.09 \pm 0.40$	$1.60 \pm 0.44$	$1.12 \pm 0.50$	$1.33 \pm 0.36$
1826	$1.78 \pm 1.62$	$0.75 \pm 0.92$	$5.46 \pm 1.59$	$3.01 \pm 0.56$	$2.78 \pm 1.26$	$2.65 \pm 0.55$	$3.09 \pm 0.59$	$2.34 \pm 0.67$	$1.56 \pm 0.49$
1861	$1.84 \pm 0.50$	$0.52 \pm 0.44$	$4.01 \pm 0.93$	$1.78 \pm 0.43$	$4.63 \pm 0.90$	$2.00 \pm 0.44$	$2.62 \pm 0.48$	$1.92 \pm 0.55$	$1.71 \pm 0.42$
1945	$2.04 \pm 0.43$	$0.88 \pm 0.37$	$2.41 \pm 0.87$	$2.29 \pm 0.40$	$4.32 \pm 0.89$	$1.66 \pm 0.43$	$1.09 \pm 0.50$	$1.17 \pm 0.57$	$1.58 \pm 0.41$
2019	$1.84 \pm 0.52$	$1.24 \pm 0.40$	$4.44 \pm 0.91$	$2.95 \pm 0.41$	$4.45 \pm 0.90$	$2.00 \pm 0.45$	$2.99 \pm 0.49$	$2.34 \pm 0.56$	$1.71 \pm 0.43$

<sup>a</sup>without subtraction of galactic light.**Table A2.** Measured line strength indices from the galactic main body of dEs (i.e., 3 to 8 arcsec radial interval) and corrected to the Lick system.

VCC no.	$H\delta_F$ Å	$H\gamma_F$ Å	Fe4383 Å	$H\beta$ Å	Fe5015 Å	$Mg_b$ Å	Fe5270 Å	Fe5335 Å	Fe5406 Å
0216	$2.46 \pm 0.38$	$1.87 \pm 0.34$	$3.22 \pm 0.80$	$2.35 \pm 0.36$	$3.13 \pm 0.84$	$2.02 \pm 0.40$	$1.61 \pm 0.46$	$1.35 \pm 0.51$	$1.16 \pm 0.38$
0308	$1.56 \pm 0.38$	$0.85 \pm 0.34$	$3.30 \pm 0.78$	$2.46 \pm 0.36$	$4.43 \pm 0.81$	$2.00 \pm 0.39$	$2.37 \pm 0.44$	$2.06 \pm 0.50$	$1.07 \pm 0.37$
0389	$-0.57 \pm 0.43$	$-0.06 \pm 0.37$	$3.26 \pm 0.79$	$2.49 \pm 0.36$	$4.10 \pm 0.81$	$2.22 \pm 0.38$	$2.48 \pm 0.43$	$1.89 \pm 0.48$	$1.21 \pm 0.37$
0490	$1.26 \pm 0.53$	$0.64 \pm 0.48$	$5.05 \pm 1.04$	$2.26 \pm 0.49$	$4.38 \pm 1.10$	$2.23 \pm 0.53$	$2.35 \pm 0.60$	$1.87 \pm 0.67$	$1.19 \pm 0.49$
0545	$-0.05 \pm 0.43$	$0.09 \pm 0.37$	$2.51 \pm 0.83$	$2.13 \pm 0.38$	$3.82 \pm 0.85$	$1.26 \pm 0.42$	$0.78 \pm 0.48$	$0.86 \pm 0.53$	$1.16 \pm 0.39$
0856	$1.39 \pm 0.35$	$-0.48 \pm 0.32$	$3.80 \pm 0.70$	$1.94 \pm 0.33$	$3.84 \pm 0.73$	$2.11 \pm 0.35$	$2.07 \pm 0.39$	$1.84 \pm 0.44$	$1.23 \pm 0.33$
0929	$1.71 \pm 0.32$	$-0.66 \pm 0.31$	$5.48 \pm 0.62$	$2.25 \pm 0.30$	$4.40 \pm 0.66$	$3.21 \pm 0.31$	$2.78 \pm 0.36$	$1.75 \pm 0.40$	$1.43 \pm 0.30$
0990	$0.88 \pm 0.35$	$0.36 \pm 0.31$	$4.18 \pm 0.66$	$2.21 \pm 0.30$	$4.52 \pm 0.70$	$2.27 \pm 0.32$	$2.12 \pm 0.37$	$1.68 \pm 0.42$	$1.31 \pm 0.32$
1167	$1.79 \pm 0.41$	$0.37 \pm 0.39$	$3.41 \pm 0.84$	$2.59 \pm 0.39$	$3.07 \pm 0.91$	$2.08 \pm 0.43$	$1.75 \pm 0.48$	$1.01 \pm 0.58$	$1.41 \pm 0.40$
1185	$1.50 \pm 0.32$	$-0.88 \pm 0.31$	$3.54 \pm 0.65$	$1.53 \pm 0.32$	$3.48 \pm 0.69$	$1.59 \pm 0.35$	$1.08 \pm 0.39$	$2.12 \pm 0.42$	$1.19 \pm 0.32$
1254	$0.60 \pm 0.45$	$-0.18 \pm 0.39$	$5.24 \pm 0.83$	$1.20 \pm 0.41$	$3.84 \pm 0.91$	$2.86 \pm 0.42$	$1.86 \pm 0.50$	$2.48 \pm 0.55$	$2.09 \pm 0.40$
1261	$1.20 \pm 0.27$	$0.40 \pm 0.25$	$3.61 \pm 0.56$	$2.03 \pm 0.26$	$3.66 \pm 0.57$	$2.38 \pm 0.28$	$2.16 \pm 0.31$	$1.51 \pm 0.36$	$1.37 \pm 0.26$
1304	$2.31 \pm 0.37$	$0.97 \pm 0.36$	$3.88 \pm 0.78$	$2.35 \pm 0.37$	$4.14 \pm 0.82$	$1.65 \pm 0.40$	$2.31 \pm 0.44$	$1.90 \pm 0.49$	$1.06 \pm 0.38$
1308	$1.72 \pm 0.43$	$0.15 \pm 0.40$	$2.38 \pm 0.91$	$1.94 \pm 0.41$	$4.91 \pm 0.93$	$2.24 \pm 0.43$	$1.86 \pm 0.50$	$2.15 \pm 0.56$	$1.16 \pm 0.43$
1333	$6.16 \pm 0.39$	$1.44 \pm 0.50$	$1.13 \pm 1.04$	$3.69 \pm 0.44$	$1.94 \pm 1.08$	$1.60 \pm 0.51$	$1.48 \pm 0.57$	$0.97 \pm 0.67$	$1.29 \pm 0.47$
1348	$2.56 \pm 0.46$	$-1.30 \pm 0.49$	$3.50 \pm 0.98$	$1.94 \pm 0.49$	$3.15 \pm 1.06$	$3.14 \pm 0.48$	$0.39 \pm 0.59$	$1.00 \pm 0.66$	$1.50 \pm 0.47$
1353	$2.37 \pm 0.37$	$1.52 \pm 0.35$	$0.42 \pm 0.85$	$2.78 \pm 0.38$	$3.08 \pm 0.86$	$2.21 \pm 0.40$	$1.78 \pm 0.46$	$1.14 \pm 0.52$	$1.43 \pm 0.40$
1355	$1.86 \pm 0.43$	$1.08 \pm 0.40$	$3.05 \pm 0.90$	$2.45 \pm 0.43$	$4.65 \pm 0.97$	$1.93 \pm 0.46$	$2.03 \pm 0.52$	$1.46 \pm 0.59$	$1.63 \pm 0.44$
1389	$1.12 \pm 0.39$	$0.18 \pm 0.37$	$2.32 \pm 0.80$	$2.15 \pm 0.38$	$2.77 \pm 0.90$	$1.83 \pm 0.42$	$1.75 \pm 0.47$	$1.19 \pm 0.54$	$0.29 \pm 0.41$
1407	$1.40 \pm 0.39$	$0.55 \pm 0.34$	$3.33 \pm 0.78$	$1.90 \pm 0.36$	$3.87 \pm 0.80$	$2.34 \pm 0.38$	$2.03 \pm 0.43$	$1.51 \pm 0.49$	$0.91 \pm 0.37$
1661	$-0.04 \pm 0.45$	$0.02 \pm 0.40$	$4.31 \pm 0.89$	$2.17 \pm 0.42$	$5.75 \pm 0.96$	$1.30 \pm 0.46$	$1.10 \pm 0.53$	$2.63 \pm 0.57$	$1.63 \pm 0.42$
1826	$1.85 \pm 0.35$	$-0.13 \pm 0.34$	$1.10 \pm 0.75$	$2.02 \pm 0.36$	$4.58 \pm 0.82$	$1.34 \pm 0.40$	$1.97 \pm 0.45$	$1.91 \pm 0.50$	$1.15 \pm 0.37$
1861	$1.32 \pm 0.39$	$-0.02 \pm 0.36$	$4.58 \pm 0.74$	$2.11 \pm 0.35$	$4.68 \pm 0.77$	$2.88 \pm 0.37$	$1.92 \pm 0.43$	$2.32 \pm 0.47$	$1.56 \pm 0.37$
1945	$1.96 \pm 0.35$	$0.94 \pm 0.33$	$6.20 \pm 0.70$	$1.66 \pm 0.36$	$2.89 \pm 0.81$	$1.59 \pm 0.39$	$1.46 \pm 0.44$	$2.09 \pm 0.49$	$1.23 \pm 0.36$
2019	$0.68 \pm 0.43$	$0.02 \pm 0.37$	$3.97 \pm 0.82$	$1.94 \pm 0.39$	$4.63 \pm 0.89$	$2.35 \pm 0.42$	$2.12 \pm 0.49$	$1.55 \pm 0.56$	$1.36 \pm 0.42$

## APPENDIX B: EXTRACTION OF SSP PARAMETERS

It is well known that the age-metallicity degeneracy is a difficult problem to estimate galaxy age and metallicity. However, there are several different methods have been suggested to cope with this complication. By using the large number of indices and adopting the technique of Proctor & Sansom (2002), the effect of this degeneracy on the estimates of SSP parameters can be minimized. Fig. B1, shows examples of the of  $\Delta\chi^2$  contours obtained with the method we have used to derive the SSP parameters, indicating the minimum with a diamond symbol. The contours are drawn with  $\Delta\chi^2 = 2.3$  (i.e., errors including 2 degrees of freedom (Press et al. 1992, Section 15.6)). This shows that the typical  $1\sigma$  uncertainties we obtain on the SSP parameters are of the order of 0.1 dex. The effect of the age-metallicity degeneracy (e.g. Worthey et al. 1994) can be recognized in the tilt of the contours in the age Vs metallicity plot.

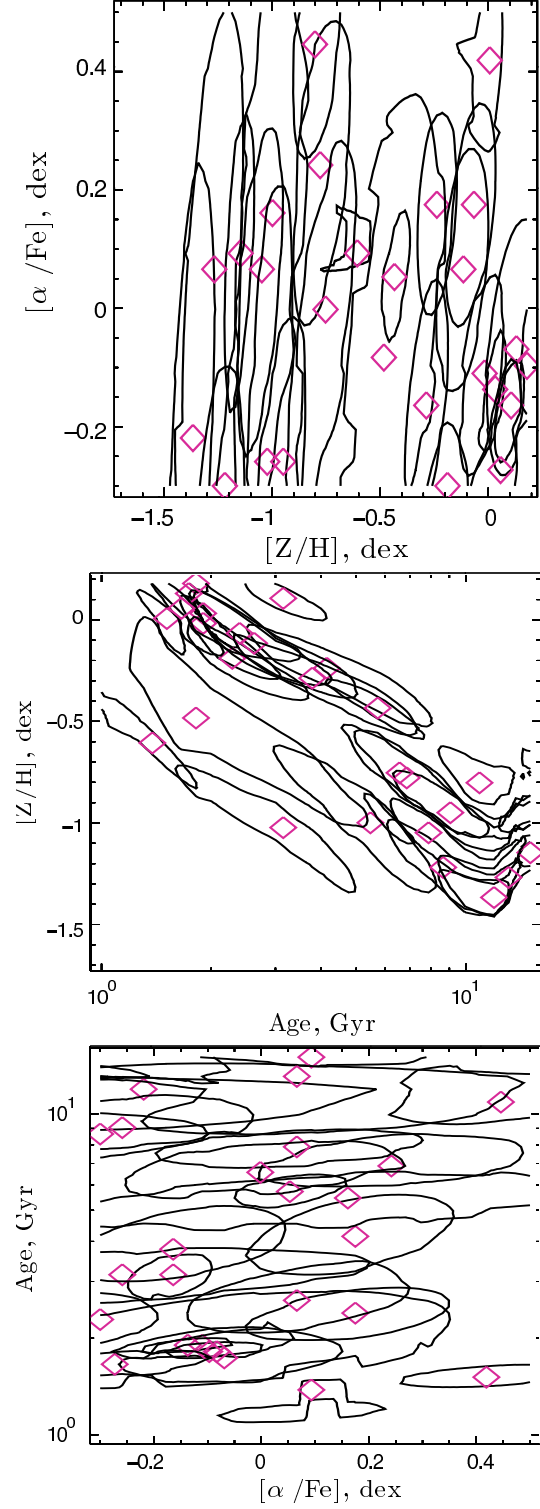


**Figure B1.** Examples of  $\Delta\chi^2$  contours in different projection planes of age, metallicity and  $[\alpha/\text{Fe}]$ -abundance space.